



2021

Populations of Major Phases in Glacier Peak Lavas

Charlotte Wall
Western Washington University

Follow this and additional works at: https://cedar.wwu.edu/geology_studentpubs



Part of the [Geochemistry Commons](#), [Geology Commons](#), and the [Geophysics and Seismology Commons](#)

Recommended Citation

Wall, Charlotte, "Populations of Major Phases in Glacier Peak Lavas" (2021). *Geology Graduate and Undergraduate Student Scholarship*. 4.
https://cedar.wwu.edu/geology_studentpubs/4

This Article is brought to you for free and open access by the Geology at Western CEDAR. It has been accepted for inclusion in Geology Graduate and Undergraduate Student Scholarship by an authorized administrator of Western CEDAR. For more information, please contact westerncedar@wwu.edu.

Populations of Major Phases in Glacier Peak Lavas

Charlotte Wall

Senior Thesis

Department of Geology

Western Washington University

Advisor: Dr. Mai Sas



ABSTRACT

Volcanoes can be studied through minerals that are present in their eruption products. These minerals can be studied through optical microscopy and geochemistry to better understand their origins and provide insight into which processes took place prior to eruption (i.e., fractionation of crystals, assimilation of the surrounding crust, magma mixing). In this study I examine mineral populations in dacite (lava of intermediate composition) from Dahkobod/Glacier Peak volcano in the north Cascade Arc. The samples consist of a felsic (high SiO₂) host component and a mafic (low SiO₂) inclusion component. To establish base mineral populations, minerals from both the host and inclusion were examined with a petrographic microscope. Then, representative crystals from each possible plagioclase, pyroxene, and olivine population were analyzed using a scanning electron microscope – electron diffusive X-ray spectroscopy (SEM-EDS) for their major element compositions. Results indicate that there are 3 sets of crystal populations, one from the felsic host (consisting of plagioclase, pyroxenes, amphibole, and quartz), one from the mafic inclusion (consisting of olivine, plagioclase, and pyroxenes), and one from an intermediate source (consisting of clusters of plagioclase and pyroxenes). Minerals in the host and inclusion all show evidence for disequilibrium re-crystallization and new crystallization following interaction. Specifically, host amphibole and quartz became unstable as evidenced by their pronounced clinopyroxene reaction rims, whereas host plagioclase and orthopyroxene continued crystallizing and nucleating as evidenced by the presence of both normally and reversely zoned crystals with overlapping compositions. In contrast, host clinopyroxene crystallized after the two magmas mingled as evidenced by normal zoning and lack of dissolution textures. Inclusion olivine became unstable after magma mingling, as evidenced by disequilibrium textures in the crystals. Inclusion plagioclase, clinopyroxene and orthopyroxene, on the other hand, crystallized after the magmas interacted and exhibit wide compositional ranges due to localized differences in the degree of magma mixing. A third set of mineral populations is present as clusters of sodic plagioclase and pyroxenes with moderate Mg contents. The origin of these clusters is unknown, but the crystal compositions did not resemble any of the established host and inclusion populations. These results suggest the magmatic system that produced the dacite samples is more complex than a two-magma system. Additionally, the mingled magmas did not erupt immediately after interacting as indicated by the continued crystallization of crystals. The exact reason for eruption is not clear; however, the host matrix is glass-rich and microcrystalline, suggesting mobilization by a new melt prior to eruption.

INTRODUCTION

Lavas consist of glasses and minerals that represent a snapshot of the magma at the time of eruption. The textures and compositions of the minerals in particular can provide information about magmatic components and pre-eruption processes that otherwise might go unrecognized (e.g., magma mixing; Streck, 2008). Investigating the volcanic minerals is especially helpful in continental arc volcanoes due to their complex nature. Continental arc volcanoes form when an oceanic plate subducts underneath a continental plate, which causes the subducting slab to dehydrate as it descends and release volatiles that aid in partial melting of the mantle (Bebout, 2013; Sparks et al., 2019). The mantle melts percolate and stagnate in the overlying continental crust, where they diversify through fractionation and assimilation, and form magma reservoirs that reside in vertically extensive systems of mush (Sparks et al., 2019). Mush is the intermediary zone between the magma and the surrounding rock and consist of solidified fragments that are surrounded by continuous melt where the melt percentage is kept relatively low (1–50%). Magma reservoirs are thought to be most concentrated just above the seismic Mohorovičić discontinuity (Moho), but multiple reservoirs can also exist in the middle and upper crust (Sparks et al., 2019). Interactions between the melts and surrounding mush result in compositional changes to both (Sparks et al., 2019). For example, a recent study of the dacitic stratovolcano Loowit/Mount St. Helens, which is located in the Cascade volcanic arc in western North America, found evidence for three distinct parental magmas (mantle melts) hosted within a mush network (Leeman and Smith 2018). Specifically, the authors determined that the parental magmas mixed both with each other and with the mush around them to create lineages that are geochemically consistent with samples collected at and near Mount St. Helens. The authors also found the mineral textures in those samples are consistent with this model of the magmatic system. Leeman and Smith (2018) demonstrate that the presence of large, long lived, and complex conduit systems underneath stratovolcanoes can result in modifications to mantle melts that travel through or stagnate in the crustal mush, which has important implications for eruption behavior. Therefore, deciphering the complexity of a magmatic system underneath a volcano, such as at Mount St. Helens, helps geoscientists better understand the hazards a volcano poses.

Dahkobod/Glacier Peak is a dacitic Cascade stratovolcano, like Mount St. Helens, and poses similar hazards (e.g., ashfall, lahars, and floods; Beget, 1983; Fig. 1, Fig. 2), but is less studied. While currently Glacier Peak is thought to be in a dormant state, historically it goes through active and dormant phases with inconsistent durations (Beget, 1983). Some mineral-based studies at Glacier Peak have helped improve our understanding of the processes occurring at this magmatic system. For example, a recent study that focused on mineral textures and geochemistry demonstrated that the Lightning Creek high-Mg basaltic andesite, a Glacier Peak lava with high Mg relative to SiO₂ contents, has at least three distinct magmatic components with two or more mineral populations of plagioclase, olivine, clinopyroxene, and orthopyroxene (Sas et al., 2017). The study determined the magmatic components to be a partial melt of a depleted mantle source, a crustally-derived dacite, and an andesite that fractionated from mantle partial melts. Similarly, in a study focusing on Glacier Peak's nearest volcanic neighbor, the Kulshan/Mount Baker Volcanic Field, Escobar-Burciaga (2016) used the compositions and textures of mineral assemblages to identify likely parental compositions. This study found evidence for

discrete magmas and complex open system processes, including magma passage through multiple crystal mushes prior to eruption. These studies show that complex open system processes are prevalent in this northern segment of the Cascade volcanic arc, and that whole rock-only studies neglect to recognize some processes that are essential for magma petrogenesis. This study aims to improve our understanding of the Glacier Peak magmatic system and pre-eruption processes by examining the petrological and geochemical attributes of silicic Glacier Peak lavas. Specifically, this study will apply a similar approach to the aforementioned studies to a dacitic Glacier Peak lava that mingled with mafic melt(s) in order to identify distinct mineral populations, the total number of mingled magmas, and which open system processes took place prior to eruption.

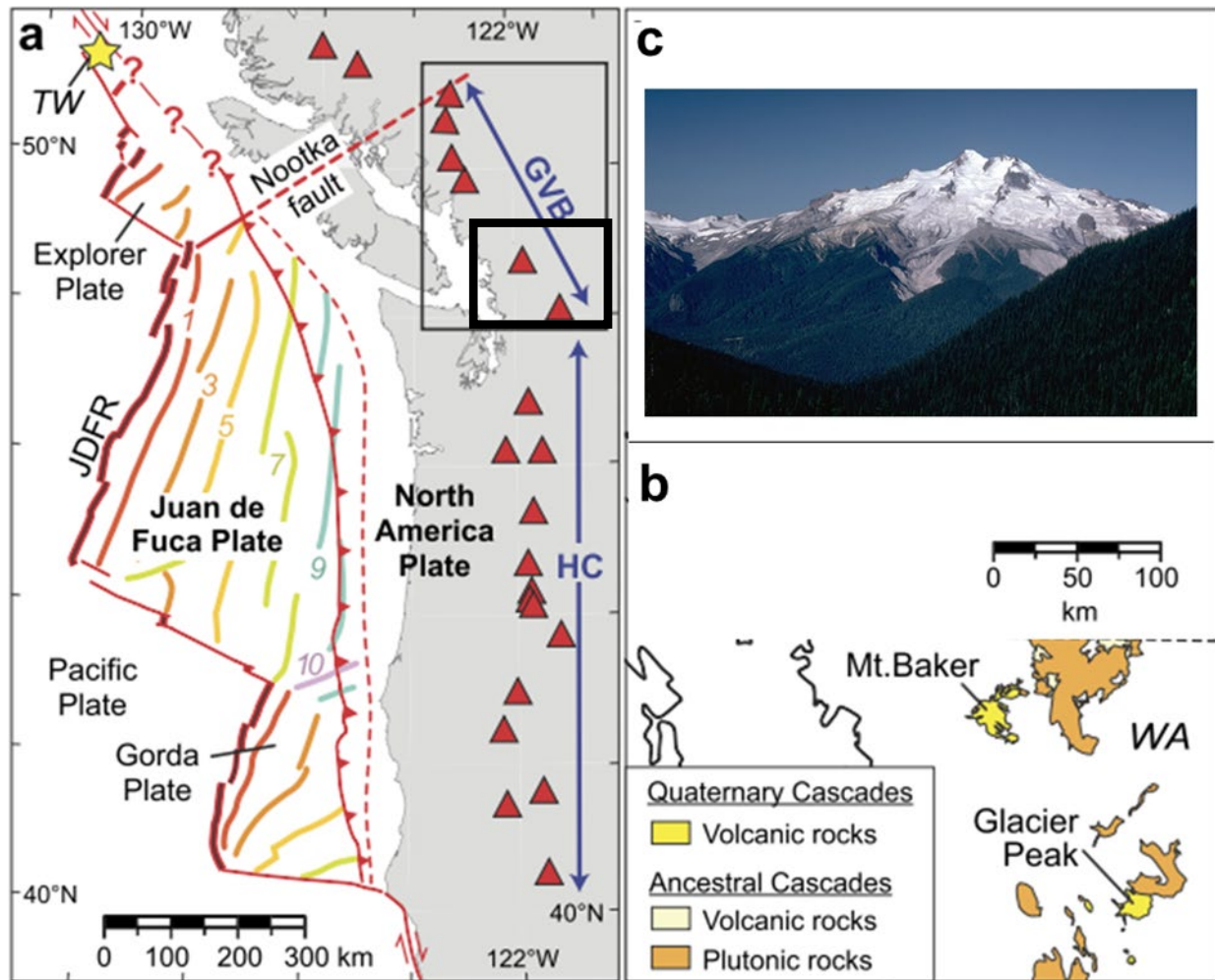


Figure 1. Map of the Cascade volcanic arc, associated subduction oceanic crust, and igneous rocks surrounding Glacier Peak. Image (a) shows the subduction zone along the west coast of western North America. Red triangles are representative of active volcanic centers, and lines along the subducting plates are the age (in Ma) of the Juan de Fuca subducting plates (JDFR is the Juan de Fuca mid ocean ridge), and the blue arrows show the extent of the high cascades (HC) and the Garibaldi Volcanic Belt (GVB). Image (b) zooms in on the area in the thick black box in of image (a), showing the volcanic and plutonic rocks of the Mount Baker and Glacier Peak volcanic centers. Image (c) is a photograph of Glacier Peak (image from the Global Volcanism Program of the Smithsonian Institute). Modified from Mullen and Weis (2015).

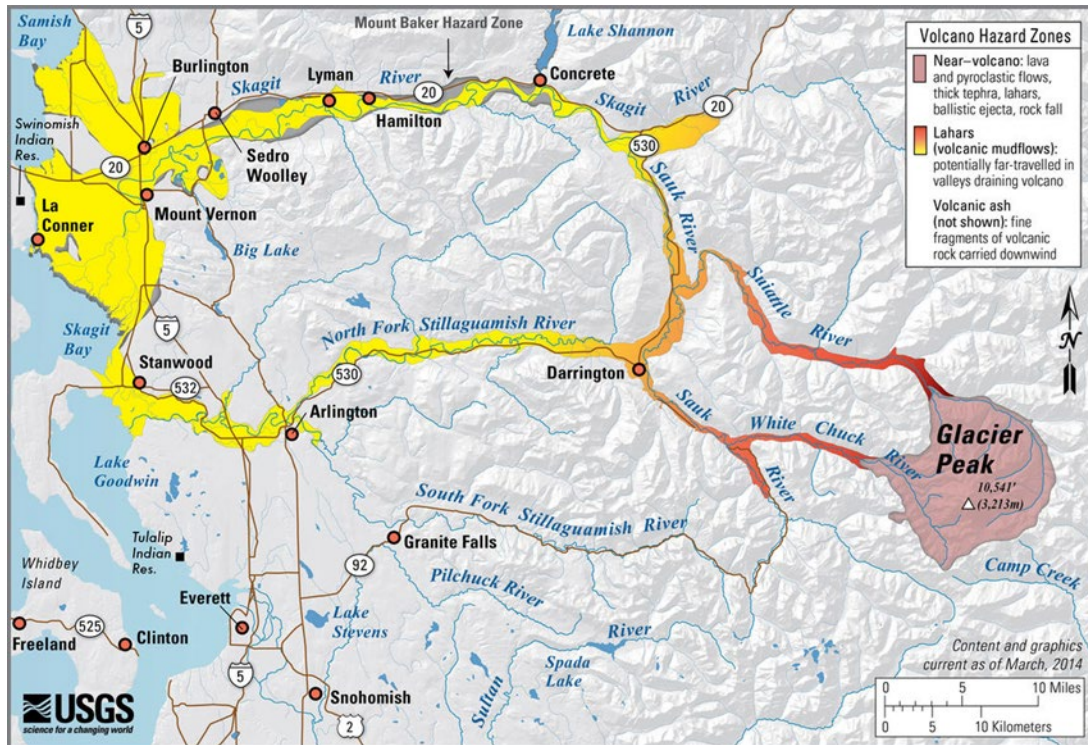


Figure 2. Map showing potential Glacier Peak hazards (United States Geologic Survey, 2018). The pale red color surrounding glacier peak is representative of the area likely to experience events like lava and pyroclastic flows, ejectas, rocks falls, tephra, etc. The red to yellow gradient is representative of the likely extent of volcanic mudflows with the most intense mudflows in red near Glacier Peak.

BACKGROUND

Glacier Peak is a 3,214 m dacitic stratovolcano that is located in the northern section of the Cascade arc, ~100 km northeast of Seattle (Fig. 1), and is one of five volcanoes that are considered active in Washington State (Beget, 1983). The Cascade arc is an active volcanic arc formed as a result of a remnant pieces of the Farallon plate (the Juan de Fuca, Explorer, and Gorda plates) subducting underneath the North American plate, and stretches from southwestern British Columbia to northern California (Fig. 1). The Cascadia trench is the subduction zone of all three plates and is less than 160 km from the coastline (DiPietro, 2018). Subduction occurs at a rate of 45 mm/yr at the northern end of the Juan de Fuca plate and 30 mm/yr on its southern boundary (McCrory et al., 2012). The slab dip in the northern part of the Juan de Fuca plate is 22° (Syracuse et al., 2010).

The age and pre-glacial (pre-15 ky) history of Glacier Peak is poorly constrained, but lava flows capping the northern and eastern ridges surrounding the volcanic edifice, which are thought to be the oldest known Glacier Peak flows, have been radiometrically dated to between 600 to 200 ky (United States Geologic Survey, 2018). Post-glacially, Glacier Peak has an active recent history of explosive eruption periods and poses a significant hazard to communities throughout Washington (Fig. 2) (Beget 1983). Older eruptions (~11–6 ky) produced tephra deposits with estimated volumes of 2.2–2.5 km³, multiple

domes, recurring pyroclastic flows (≥ 10 occurrences), and many lahars that traveled >100 km downstream during a single period of activity (Beget, 1983). More recent eruptions (2 ky–present) produced smaller tephra deposits (10–30 cm thick on the flanks of the volcano) and fewer pyroclastic flows and lahars, although the lahars reached distances >30 km downstream that pose significant hazards to communities near the White Chuck River and the Suiattle River (Beget, 1983).

METHODS

Samples and Optical Microscopy

Dacite lava samples were collected at five sites near the summit of Glacier Peak, two to the south and three to the northeast (Fig. 3), by a previous Western Washington University graduate student. Thirty thin section slides from the five sites were examined using a Leica DM 750p petrographic microscope. Tentative populations of plagioclase, orthopyroxene, clinopyroxene, olivine, amphibole, quartz, and oxides were established based on mineral textures, and representative crystals for the plagioclase, pyroxenes, and olivine populations were chosen to be analyzed for their compositions and to confirm and/or consolidate the populations.

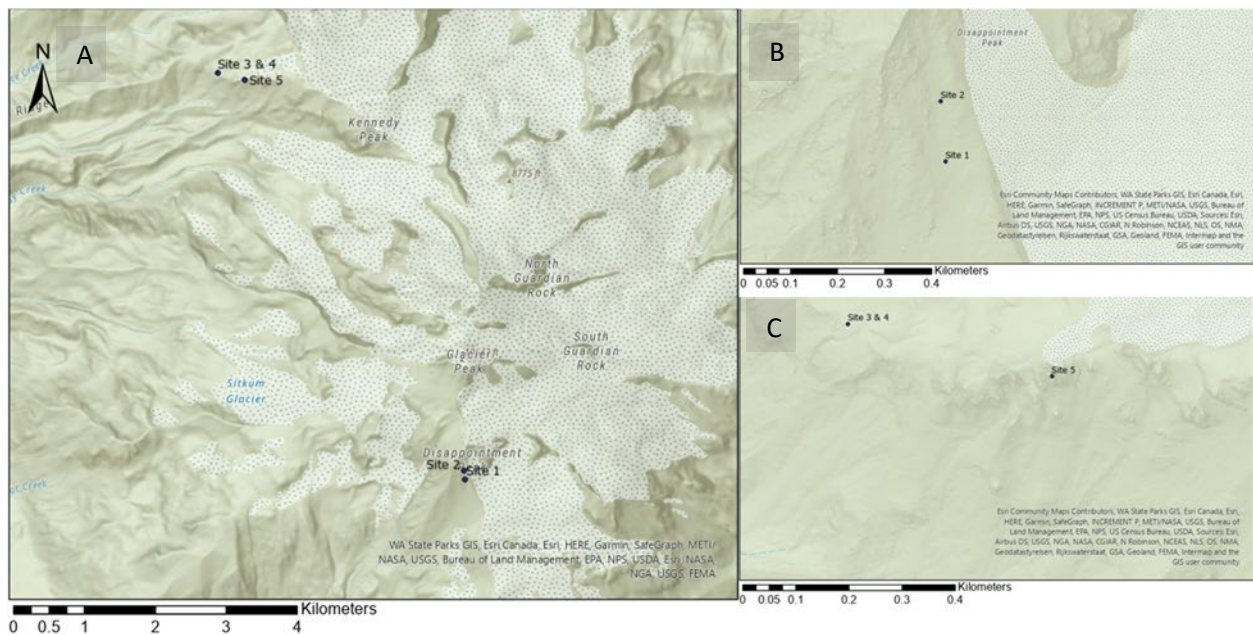


Figure 3. Map showing site locations for samples used. (A) Shows sites 1–5 in relation to Glacier Peak. (B) Shows a zoom in of sites 1 and 2. (C) Shows a zoom in of sites 3–5.

Energy Dispersive X-ray Spectroscopy

Mineral compositions were acquired through scanning electron microscope – energy dispersive X-ray spectroscopy (SEM-EDS). Crystals from seven representative slides were analyzed with a JEOL 7200 F field emission (FE)-SEM using a 150 mm² Oxford X-Max retractable EDS and a Deben high-angle annular dark field scanning transmission electron microscope (SEM-STEM) detector. Mineral images were obtained using a backscattered electron (BSE) detector. The working distance was 10 mm, the accelerating voltage was 20 kV. The chamber pressure was kept between -4 and -5 Pa and the emission current was ~66 μ A. Copper tape was used for beam calibration and AzTec software was used in conjunction with the SEM-EDS. Some of the slides were previously coated with an unknown thickness of palladium, while others were coated in 50 nm of carbon.

Back Scattered Electron Imaging and Elemental Mapping

Compositional maps were acquired using the Tescan Vega 3 Thermionic SEM, a tungsten filament SEM with an additional low vacuum Secondary Electron Tescan Detector. Element maps were created for Na, Mg, Al, Si, K, Ca, Ti, and Fe across a given field of view and the element maps could be viewed as individual elements or layered on top of one another. No quantitative data were taken from the element maps, but they aided in confirming the mineral types and zoning patterns.

RESULTS

Petrography

The samples are porphyritic dacite (host magma) with common sparsely porphyritic mafic inclusion blebs (0.5 cm – many cm in hand sample). The dacite phenocrysts (20–30%) consist of plagioclase, orthopyroxene, clinopyroxene, amphiboles, Fe-Ti oxides, and rare quartz. The dacite groundmass is fine grained, hypocrystalline with about equal amounts of microphenocrysts and glass, and the microphenocrysts are mostly plagioclase but also consist of pyroxenes and Fe-Ti oxides. The mafic inclusion consists of olivine phenocrysts (~3%), which are found in the dacite as xenocrysts (~1%), as well as pyroxene crystals (~2%) that are texturally identical to dacite pyroxenes. The mafic inclusion groundmass is holocrystalline with coarse-grained plagioclase. Lightly to severely reacted dacite phenocrysts are found throughout the mafic inclusion blebs. Table 1 provides a petrographic summary of the samples.

Plagioclase

Plagioclase crystals in the host are 0.5–8.0 mm in size and up to ~12% of the samples. The crystals are dominantly euhedral and tabular with oscillatory zoning (Fig. 4). Sieving is common among the plagioclase but ranges in severity from crystals that are barely sieved to crystals that show severe sieving. Both Carlsbad twinning and polysynthetic twinning are common in the plagioclase crystals. Plagioclase crystals are also occasionally clumped together or found in clumps with pyroxenes.

Orthopyroxene

Orthopyroxene crystals in the host are 0.2–2.0 mm in size and up to 1% of the samples. Crystals are euhedral to subhedral and elongate to prismatic in shape (Fig. 5). Orthopyroxene crystals do not exhibit twinning or obvious textural zoning. These crystals are sometimes found clumped with plagioclase or clinopyroxene and plagioclase.

Clinopyroxene

Clinopyroxene crystals in the host are 0.2–1.5 mm and up to 2% of the samples. Crystals are subhedral to anhedral and blocky in shape (Fig. 6). The clinopyroxene crystals have simple and polysynthetic twinning but no obvious textural zoning. These crystals are sometimes found clumped with plagioclase or with orthopyroxene and plagioclase.

Amphibole

Amphibole crystals in the host are 0.2–5.0 mm and up to 2% of the samples. Crystals are euhedral to subhedral and bladed or prismatic in shape (Fig. 7). Some crystals are fully reacted into clinopyroxene, others show a very prominent oxidation ring. Less reacted amphibole crystals commonly have simple twinning but no apparent zoning. More reacted crystals did not show any twinning or obvious zoning.

Quartz

Quartz crystals up to 2.0 mm are rarely (<< 1%) found throughout the samples. Crystals are subhedral to anhedral with pronounced clinopyroxene reaction rims and no zoning or twinning (Fig 8).

Oxides

Oxide crystals are common microphenocrysts and consist of blocky Fe-Ti oxides and acicular ilmenite.

Mineral Clusters

Most mineral clusters contain plagioclase with or without orthopyroxene and/or clinopyroxene (Fig. 9A–F), although some clusters contain just clinopyroxene (Fig. 9G). There is no apparent textural difference between the host and the cluster plagioclase and pyroxenes.

Mafic Inclusion Minerals

Plagioclase crystals found in inclusion blebs are 0.01–0.5 mm and straddle the microphenocryst to phenocryst boundary and make up the majority of the holocrystalline inclusion, but larger plagioclase crystals are up to 45% of the blebs. Crystals are euhedral to subhedral and tabular laths in shape and with abundant Carlsbad and polysynthetic twinning as well as oscillatory zoning (Fig. 10). Clumps of inclusion plagioclase are commonly found throughout the host. Olivine crystals found in inclusions blebs are 0.2–1.0 mm and less than 3%. Crystals are subhedral to anhedral and hexagonal and equant in shape (Fig. 11). Oxide inclusions (likely chromite) are common in the olivine crystals. Rare, heavily reacted olivine crystals are found in the host. Orthopyroxene, and clinopyroxene that are texturally identical to host minerals are sporadically found in inclusion.

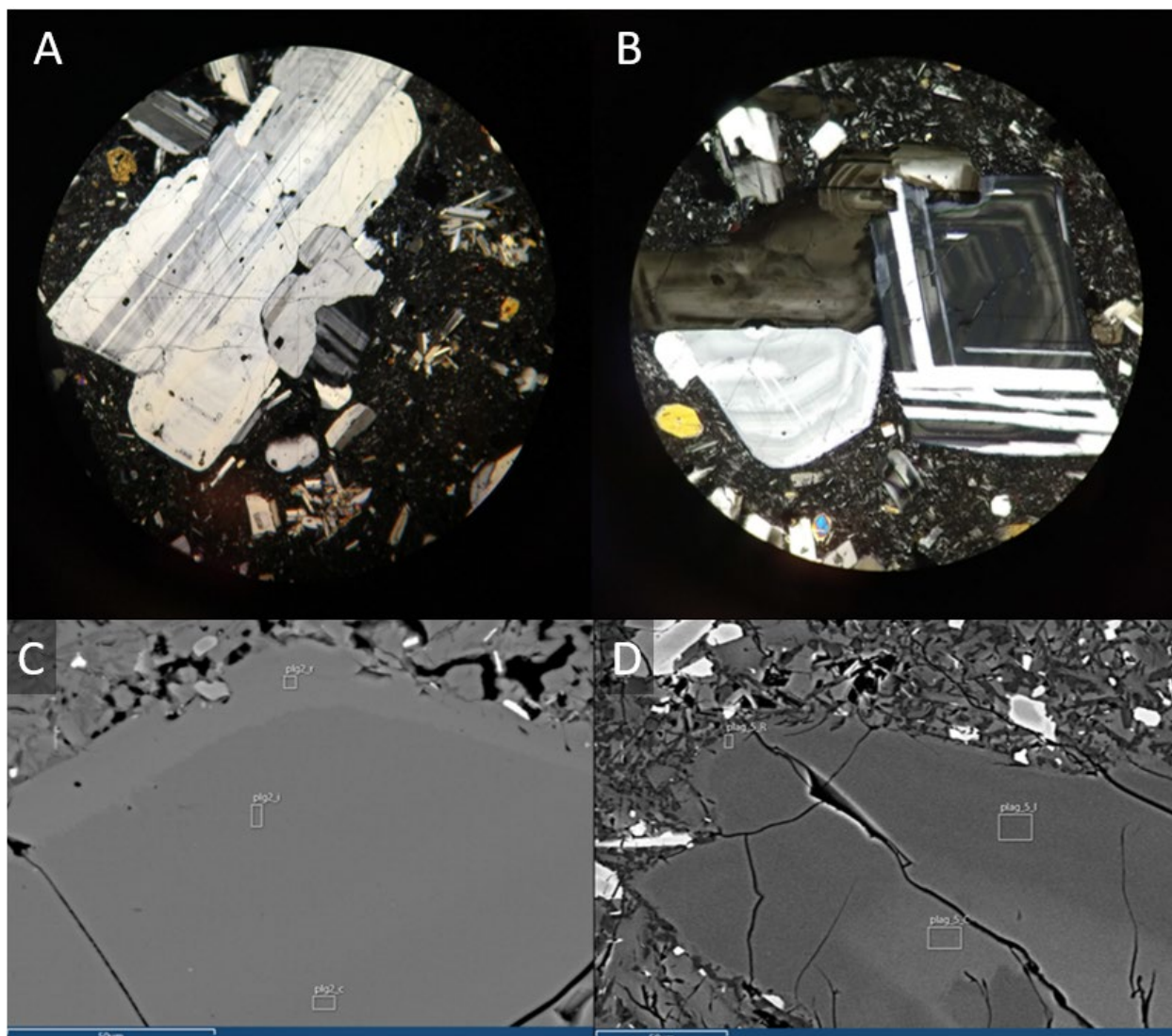


Figure 4. Petrographic and BSE images of plagioclase crystals in Glacier Peak samples. (A-B) Petrographic images of plagioclase taken with personal mobile device. Both images were taken in cross-polarized light (XPL). (C-D) BSE images of plagioclase crystals analyzed using FE-SEM, with core, mantle, and rim analysis locations marked.

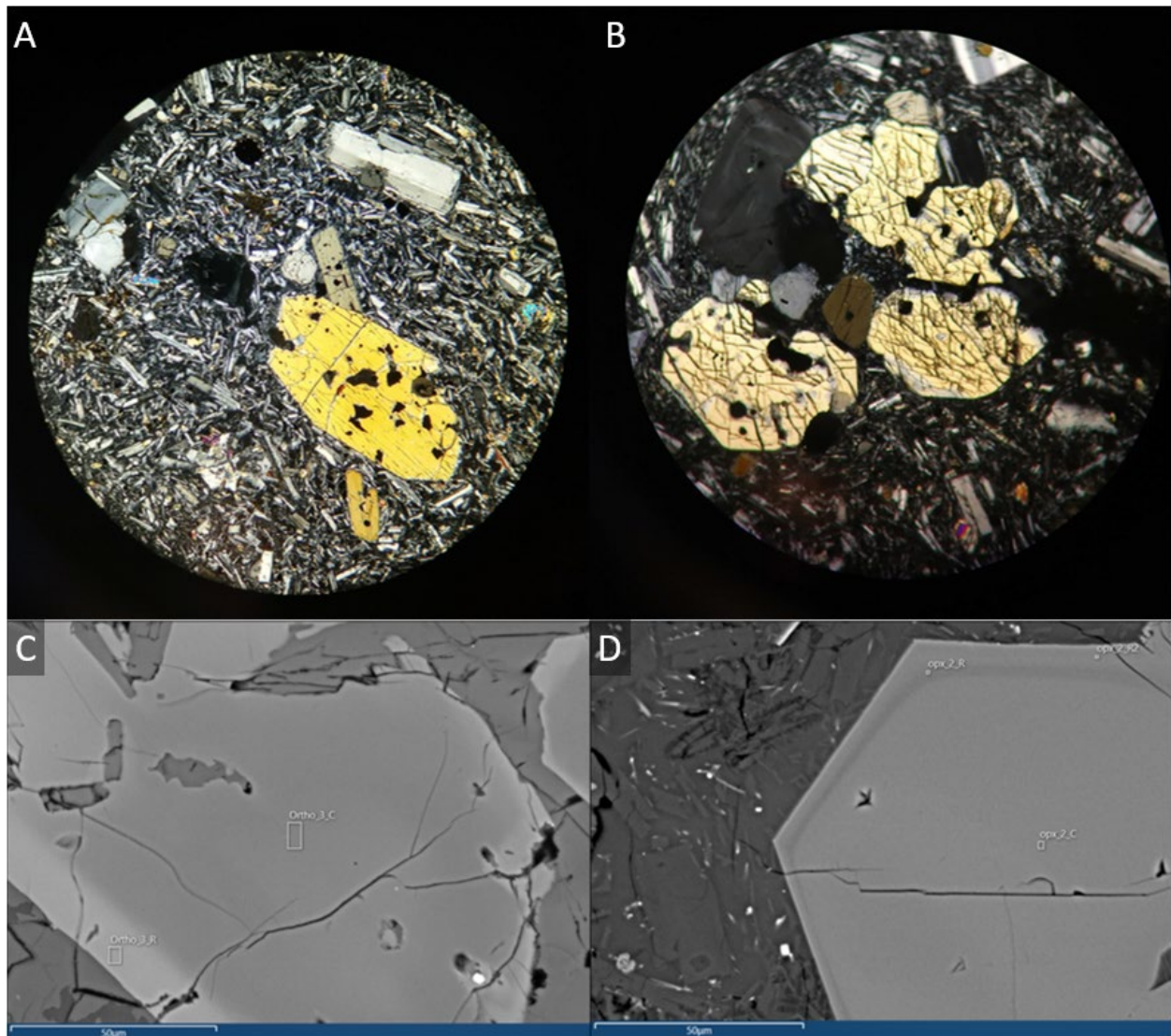


Figure 5. Petrographic and BSE images of orthopyroxene crystals in Glacier Peak samples. (A-B) Petrographic images of orthopyroxene taken with personal mobile device. Both images were taken in cross-polarized light (XPL). (C-D) BSE images of orthopyroxene crystals analyzed using FE-SEM, with core and rim analysis locations marked.

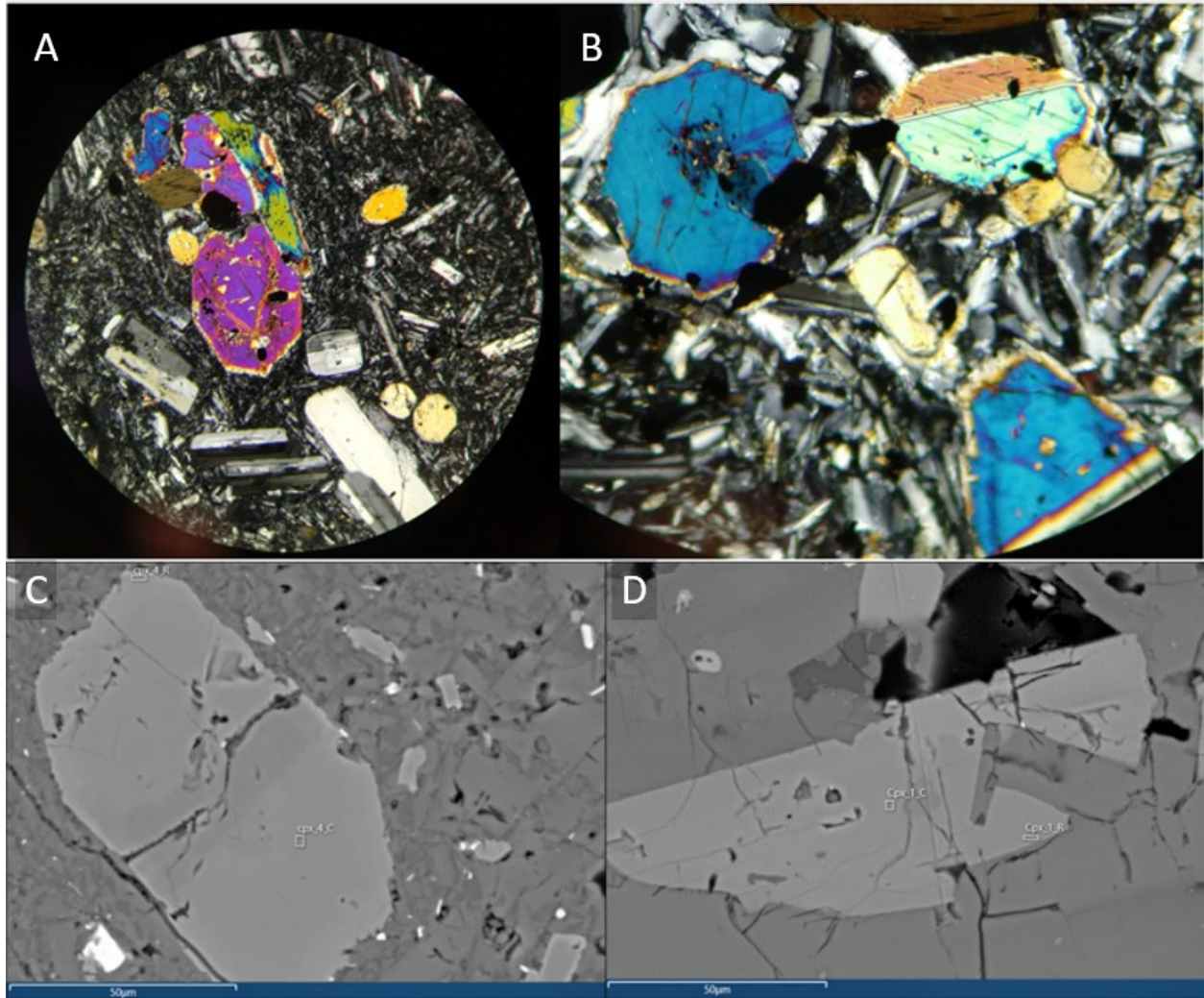


Figure 6. Petrographic and BSE images of clinopyroxene crystals in Glacier Peak samples. (A-B) Petrographic images of clinopyroxene taken with personal mobile device. Both images were taken in cross-polarized light (XPL). (C-D) BSE images of clinopyroxene crystals analyzed using FE-SEM, with core and rim analysis locations marked.

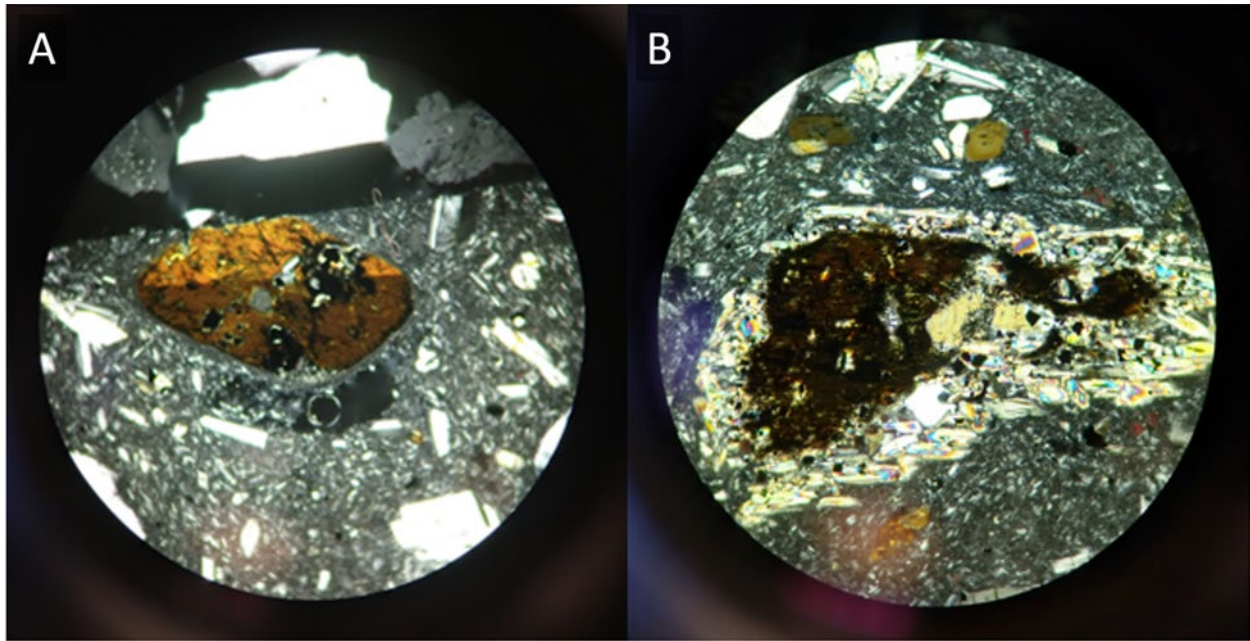


Figure 7. Petrographic images of amphibole crystals in Glacier Peak samples. (A-B) Petrographic images of amphibole taken with personal mobile device. Both images were taken in cross-polarized light (XPL). Image A shows an amphibole with a prominent oxidation ring and simple twinning, and image B shows an amphibole crystal that has partially reacted into clinopyroxene.

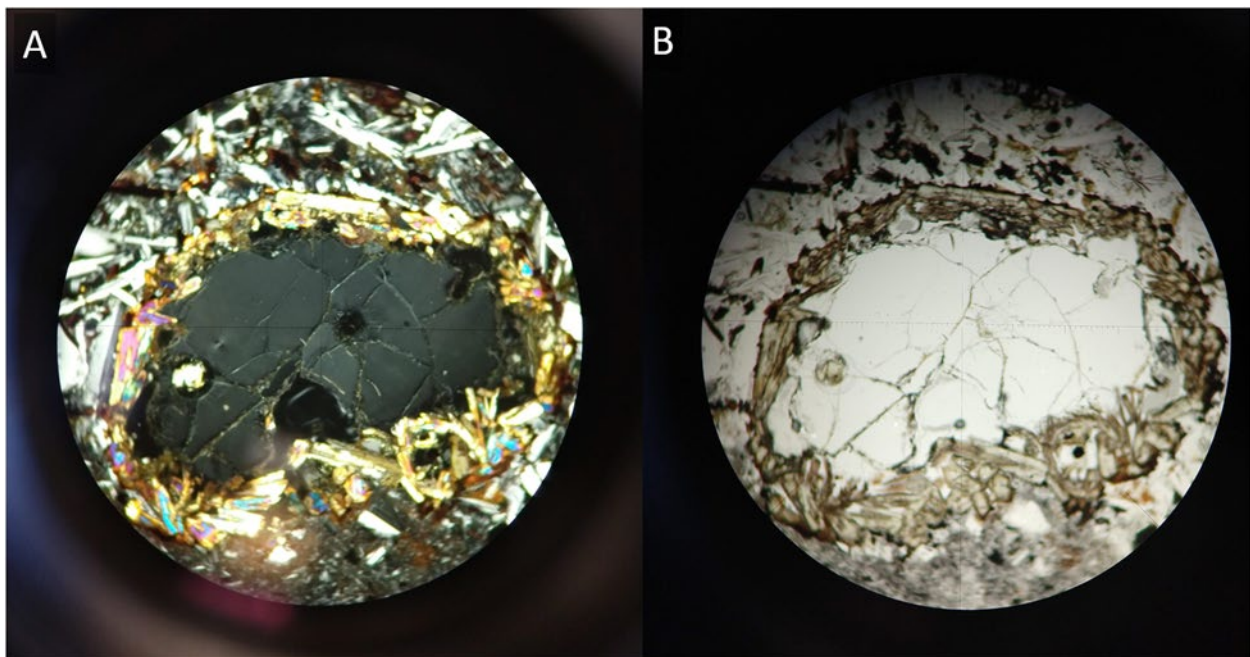


Figure 8. Petrographic images of a quartz crystal in Glacier Peak samples. Image A is the crystal in cross polarized light (XPL) and image B is the crystal in plain polarized light (PPL). The quartz crystal has a reaction ring of clinopyroxene.

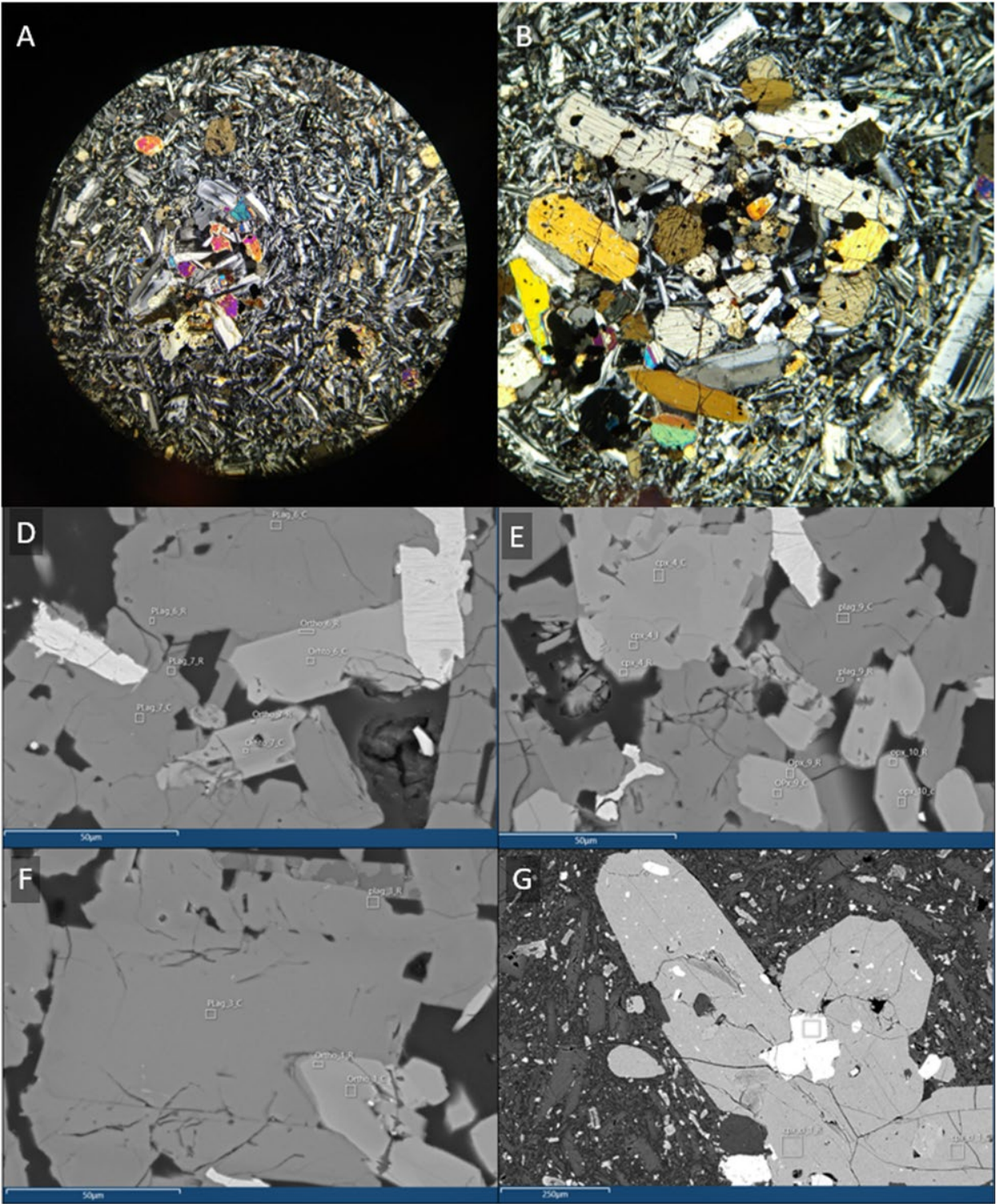


Figure 9. Petrographic and BSE images of crystal clusters in Glacier Peak samples. (A-C) Petrographic images of clusters taken with personal mobile device. Both images were taken in cross-polarized light (XPL). (D-G) BSE images of cluster crystals analyzed using SEM-EDS, with core, and rim analysis locations marked. Images A and C are clinopyroxene and plagioclase clusters, images B and E are clinopyroxene, orthopyroxene, and plagioclase clusters, images D and F are orthopyroxene and plagioclase clusters, and image G is a clinopyroxene cluster. Images A-G all depict Cluster 2 type, image F depicts Cluster 1 type.

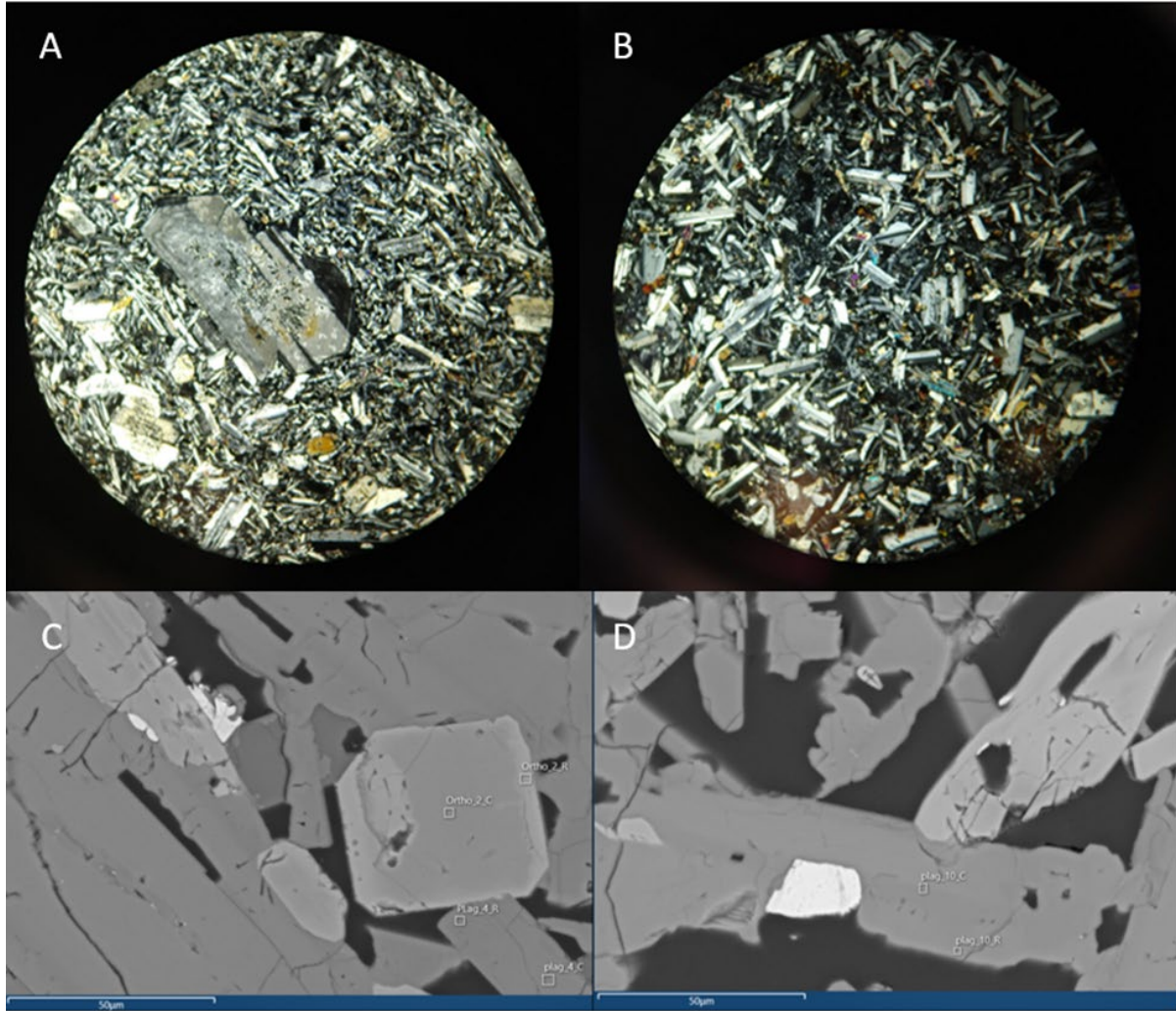


Figure 10. Petrographic and BSE images of plagioclase crystals in inclusion Glacier Peak samples. (A-B) Petrographic images of plagioclase taken with personal mobile device. Both images were taken in cross-polarized light (XPL). (C-D) BSE images of plagioclase crystals analyzed using FE-SEM, with core and rim analysis locations marked.

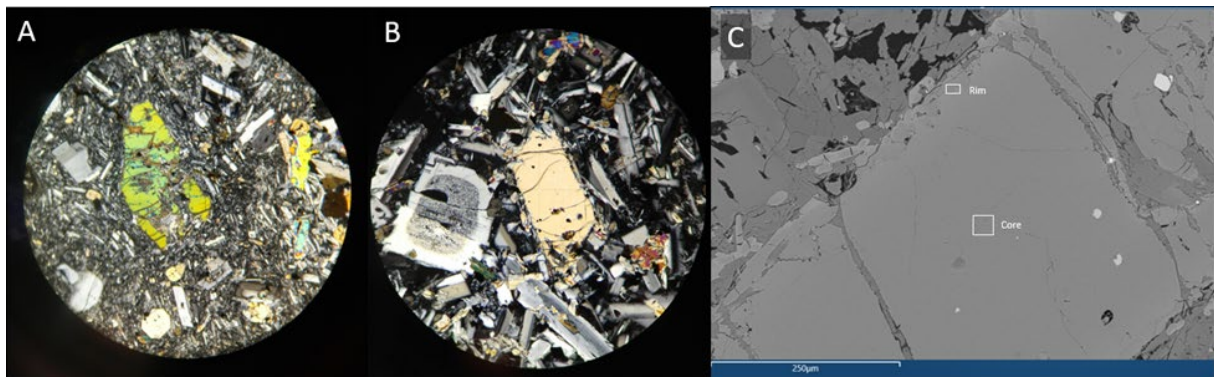


Figure 11. Petrographic and BSE images of olivine crystals in Glacier Peak samples. (A-B) Petrographic images of olivine taken with personal mobile device. Both images were taken in cross-polarized light (XPL). (C) BSE images of olivine crystals analyzed using FE-SEM, with core and rim analysis locations marked.

Mineral Compositions

Anorthite (An, molar Ca/Ca+Na+K) contents of plagioclase crystals from the host, clusters and inclusion are shown in Figure 12. Magnesium numbers (Mg#, molar Mg/Mg+Fe) of orthopyroxene crystals from the host, cluster, and host-like orthopyroxene found in the inclusion are shown in Figure 13.

Clinopyroxene crystals Mg# from the host, cluster, and host-like clinopyroxene found in the inclusion are shown in Figure 14. Forsterite (Fo, molar Mg/Mg+Fe) contents of olivine crystals from the inclusion are shown in Figure 15.

Potential Source of Error

The thin sections used in analysis were acquired and prepared by a previous graduate student, with several thin sections being previously coated using an unknown medium and thickness. During FE-SEM analyses, it was determined that some of the thin section slides were previously coated in palladium. Since the samples were coated in an unknown thickness of palladium, the settings were changed for each individual slide to produce the most consistent results. Additionally, all analyses, regardless of coating, were normalized to 100% to try and minimize inconsistencies in the sum of oxide percentages across the slides. Furthermore, any analyses that were potentially contaminated (e.g., rim analyses extending into adjacent crystals or matrix) were omitted. Some initial analyses that only included mantles of crystals (no core and/or rim analyses) were also omitted as they could not be correlated to specific mineral populations and did not contribute to the interpretations.

Host

Plagioclase

Plagioclase compositions are listed in Table 2 and shown in Figure 12. Plagioclase cores, middles, and rims exhibit significant overlap in compositions. An contents in the cores are 57–91 (n = 10), in the mantles 56–60 (n = 5), and in the rims 63–81 (n = 10). Crystals found in the host exhibit both normal (higher An contents in core versus rim) and reverse (lower An contents in cores versus rims) zoning (Fig. 12). Cores have Al₂O₃ = 24.12–32.93 wt.%, mantles have 25.60–26.87 wt.%, and rims have 26.01–30.53 wt.%. Cores have FeO = 0.32–0.77 wt.%, mantles have 0.34–0.4 wt.%, and rims have 0.61–0.84 wt.%. Cores have MgO = 0.02–0.13 wt.%, mantles have 0.03–0.16 wt.%, and rims have 0.00–0.10 wt.%. Cores have CaO = 7.92–16.70 wt.%, mantles have 7.98–8.40 wt.%, and rims have 9.20–13.79 wt.%. Cores have Na₂O = 1.76–6.61 wt.%, mantles have 5.78–6.70 wt.%, and rims have 3.28–5.70 wt.%. Cores have K₂O = 0.04–0.95 wt.%, mantles have 0.45–0.60 wt.%, and rims have 0.17–0.48 wt.%. Cores have SrO = 0.16–0.63 wt.%, mantles have 0.17–0.69 wt.%, and rims have 0.11–0.74 wt.%.

Orthopyroxene

Orthopyroxene compositions are listed in Table 3 and shown in Figure 13. Orthopyroxene core and rims exhibited some overlap in compositions. Core Mg# are 63–81 (n = 11), and in the rim 61–75 (n = 11). Crystals in the host exhibit both normal (higher Mg# in core than in rim) and reverse (lower Mg# in core than in rim) zoning. Cores have Al₂O₃ = 0.59–2.27 wt.%, and rims have 1.03–3.27 wt.%. Cores have FeO = 11.81–22.94 wt.%, rims have 16.03–22.44 wt.%. Cores have MgO = 22.16–29.18 wt.%, rims have 19.30–26.59 wt.%. Cores have CaO = 0.67–2.21 wt.%, rims have 1.33–2.33 wt.%. Cores have Na₂O = 0.01–0.15 wt.%, rims have 0.06–0.52 wt.%. Cores have K₂O = 0.00–0.07 wt.%, rims have 0.01–0.62 wt.%. Cores have SrO = 0.02–0.21 wt.%, rims have 0.00–0.23 wt.%.

Clinopyroxene

Clinopyroxene compositions are listed in Table 4 and shown in Figure 14. Clinopyroxene core and rims showed some compositional overlap. Cores have Mg# 74–80 (n = 6), rims have 62–74 (n = 6). All clinopyroxene crystals in the host exhibited normal zoning. Cores have Al₂O₃ = 0.95–4.4 wt.%, rims have 0.90–3.96 wt.%. Cores have FeO = 7.5–8.89 wt.%, rims have 8.87–22.05. Cores have MgO = 14.27–17.12 wt.%, rims have 13.5–20.42 wt.%. Cores have CaO = 18.89–22.09 wt.%, rims have 1.77–21.95 wt.%. Cores have Na₂O = 0.24–0.40 wt.%, rims have 0.32–0.69 wt.%. Cores have K₂O = 0.00–0.04 wt.%, rims have 0.04–0.09 wt.%. Cores have SrO = 0.00–0.47 wt.%, rims have 0.00–0.44 wt.%.

Clusters

Plagioclase

Only cores of plagioclase crystals in clusters were analyzed (Table 2, Fig. 12). Plagioclase crystals found in clusters have core An contents 6–83 (n = 5), Al₂O₃ = 1.85–31.74 wt.%, FeO = 0.17–1.20 wt.%, MgO = 0.03–0.17 wt.%, CaO = 0.10–14.53 wt.%, Na₂O = 0.94–7.31 wt.%, K₂O = 0.00–9.44 wt.%, and SrO = 0.00–0.22 wt.%.

Orthopyroxene

Orthopyroxene crystals found in clusters have differing core and rims compositions (Table 3, Fig. 13). Cores have Mg# 74–75 (n = 2), rims have Mg# 58 (n = 1). Orthopyroxene crystals in clusters exhibit normal zoning. Core Al₂O₃ = 2.39–2.92 wt.%, rim Al₂O₃ = 0.55 wt.%. Core FeO = 15.72–16.50 wt.%, rim FeO = 24.46 wt.%. Core MgO = 25.70–26.5 wt.% and rim MgO = 19.17wt.%. Core CaO = 1.81–1.93 wt.% and rim CaO = 1.43 wt.%. Core Na₂O = 0.07–0.09 wt.% and rim Na₂O = 0.15 wt.%. Core K₂O = 0.01–0.03 wt.% and rim K₂O = 0.07 wt.%. Core SrO = 0.00–0.03 wt.%, rim SrO = 0.00 wt.%.

Clinopyroxene

Clinopyroxene crystals found in clusters have overlap in core and rim compositions (Table 4, Fig. 14). Cores have Mg# 74–81 (n = 13) and rims have 71–73 (n = 2). Clinopyroxene crystals in clusters are normally zoned. Cores have Al₂O₃ = 1.24–5.41 wt.%, and rims have 2.61–2.71 wt.%. Cores have FeO = 7.37–16.16 wt.% and rims have 9.36–16.72 wt.%. Cores have MgO = 14.57–26.46 wt.% and rims have 14.26–23.40 wt.%. Cores have CaO = 1.62–21.72 wt.% and rims have 2.24–19.57 wt.%. Cores have Na₂O = 0.04–0.50 wt.% and rims have 0.10–0.57 wt.%. Cores have K₂O = 0.00–0.14 wt.% and rims have 0.07–0.25 wt.%. Cores have SrO = 0.00–0.20 wt.% and rims have 0.04–0.06 wt.%.

Mafic Inclusion

Olivine

Olivine compositions are listed in Table 5 and shown in Figure 15. Olivine core and rim compositions have slight overlap. Fo contents in olivine cores are 81–83 (n = 3), mantles are 82 (n = 1), and rims are 59–80 (n = 2). Olivine crystals exhibit normal zoning. Cores have Al₂O₃ = 0.00–0.90 wt.%, mantles have 0.05 wt.%, and rims have 0.09–2.80 wt.%. Cores have FeO = 12.43–16.50 wt.%, mantles have 16.57 wt.%, and rims have 18.78–20.83 wt.%. Cores have MgO = 29.25–43.70 wt.%, mantles have 43.55 wt.%, and rims have 17.09–41.67 wt.%. Cores have CaO = 0.13–1.78 wt.%, mantles have 0.14 wt.%, and rims have 0.13–1.91wt.%. Cores have Na₂O = 0.03–0.12 wt.%, mantles have 0.08 wt.%, and rims have 0.01–

0.60 wt.%. Cores have $K_2O = 0.02\text{--}0.03$ wt.%, mantles have 0.02 wt.%, and rims have 0.00–1.07 wt.%. Cores have $SrO = 0.08\text{--}0.11$ wt.%, mantles have 0.01 wt.%, and rims have 0.15–0.19 wt.%.

Plagioclase

Plagioclase crystals in the inclusion have distinct rim and core compositions (Table 2, Fig. 12). Core An contents are 51–78 and rims An contents are 8–39. Plagioclase crystals in the inclusion are normally zoned. Cores have $Al_2O_3 = 25.34\text{--}30.23$ wt.%, rims have 17.54–23.44 wt.%. Cores have $FeO = 0.36\text{--}1.01$ wt.%, rims have 0.35–0.78 wt.%. Cores have $MgO = 0.00\text{--}0.08$ wt.%, rims have 0.00–0.12 wt.%. Cores have $CaO = 6.78\text{--}12.86$ wt.%, rims have 0.86–4.80 wt.%. Cores have $Na_2O = 3.93\text{--}6.87$ wt.%, rims have 4.96–8.44 wt.%. Cores have $K_2O = 0.25\text{--}0.92$ wt.%, rims have 1.04–7.98 wt.%. Cores have $SrO = 0.08\text{--}0.32$ wt.%, rims have 0.00–0.15 wt.%.

Orthopyroxene

Orthopyroxene core and rim compositions in the inclusion show overlap as well (Table 3, Fig. 13). Cores have Mg# 61–82 ($n = 10$), rims have 56–68 ($n = 10$). Cores have $Al_2O_3 = 0.58\text{--}2.88$ wt.%, rims have 0.35–1.87 wt.%. Cores have $FeO = 11.46\text{--}23.61$ wt.%, rims have 19.26–25.79 wt.%. Cores have $MgO = 20.45\text{--}29.72$ wt.%, rims have 18.73–23.45 wt.%. Cores have $CaO = 1.34\text{--}2.20$ wt.%, rims have 1.39–1.84 wt.%. Cores have $Na_2O = 0.00\text{--}0.12$ wt.%, rims have 0.06–0.28 wt.%. Cores have $K_2O = 0.00\text{--}0.05$ wt.%, rims have 0.00–0.19 wt.%. Cores have $SrO = 0.00\text{--}0.24$, rims have 0.00–0.19 wt.%.

Clinopyroxene

Clinopyroxene cores and rims in the inclusion have overlapping compositions (Table 4, Fig. 14). Core Mg# 68–82 ($n = 6$), rims have 69–74 ($n = 6$). Cores have $Al_2O_3 = 1.00\text{--}4.98$ wt.%, rims have 1.09–3.10 wt.%. Cores have $FeO = 6.43\text{--}11.42$ wt.%, rims have 9.50–11.48 wt.%. Cores have $MgO = 13.93\text{--}16.32$ wt.%, rims have 14.31–15.35 wt.%. Cores have $CaO = 19.54\text{--}21.21$ wt.%, rims have 18.97–20.21 wt.%. Cores have $Na_2O = 0.25\text{--}0.41$ wt.%, rims have 0.32–0.45 wt.%. Cores have $K_2O = 0.01\text{--}0.05$, rims have 0.01–0.07 wt.%. Cores have $SrO = 0.00\text{--}0.15$, rims have 0.00–0.14 wt.%.

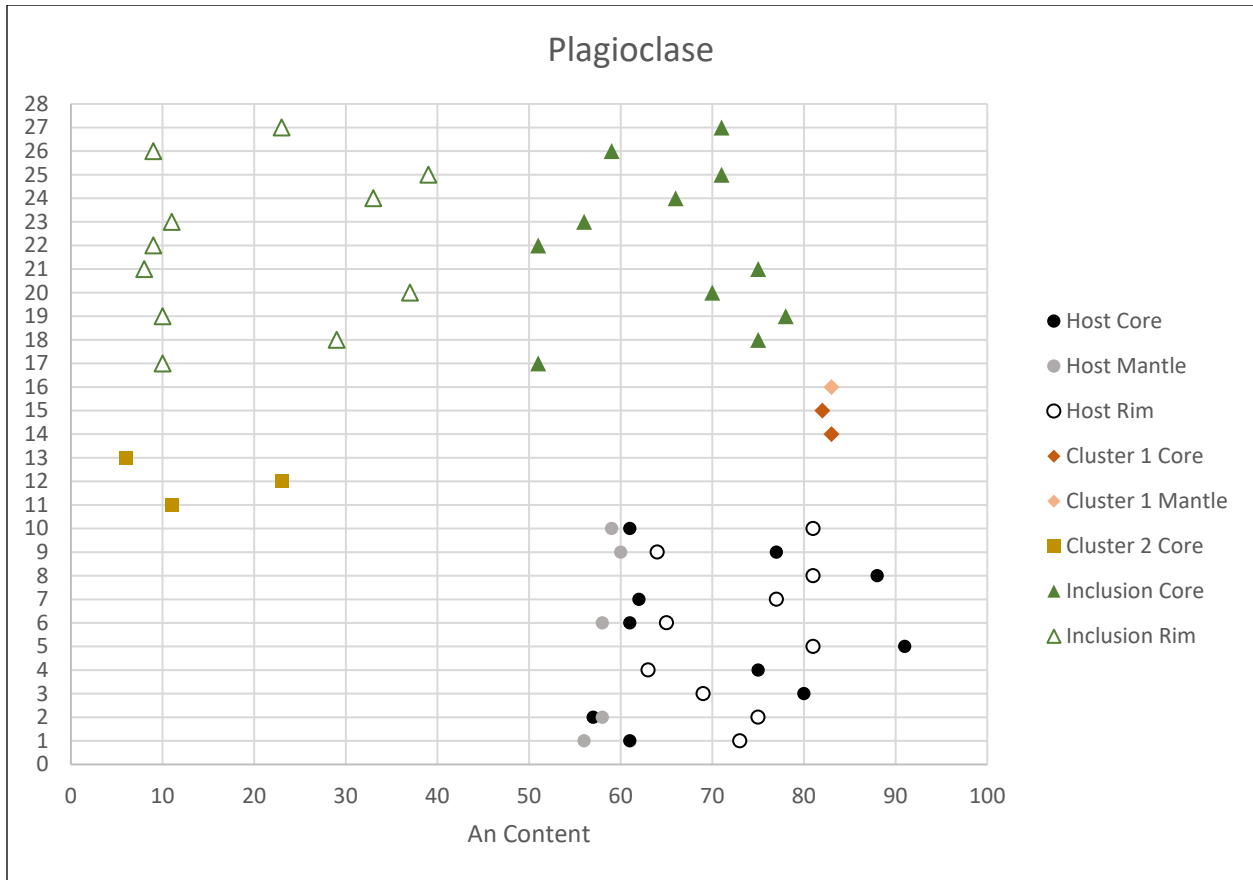


Figure 12. Plagioclase core, mantle and rim An contents of each analyzed crystals, with each line representing a single crystal. Dark, filled in shapes represent core data, light, filled in shapes represent mantle data, and outlined shapes represent rim data. Host crystals are represented as black and grey circles. Cluster crystals are represented with orange diamonds (Cluster 1) and yellow squares (Cluster 2). Inclusion crystals are represented with green triangles.

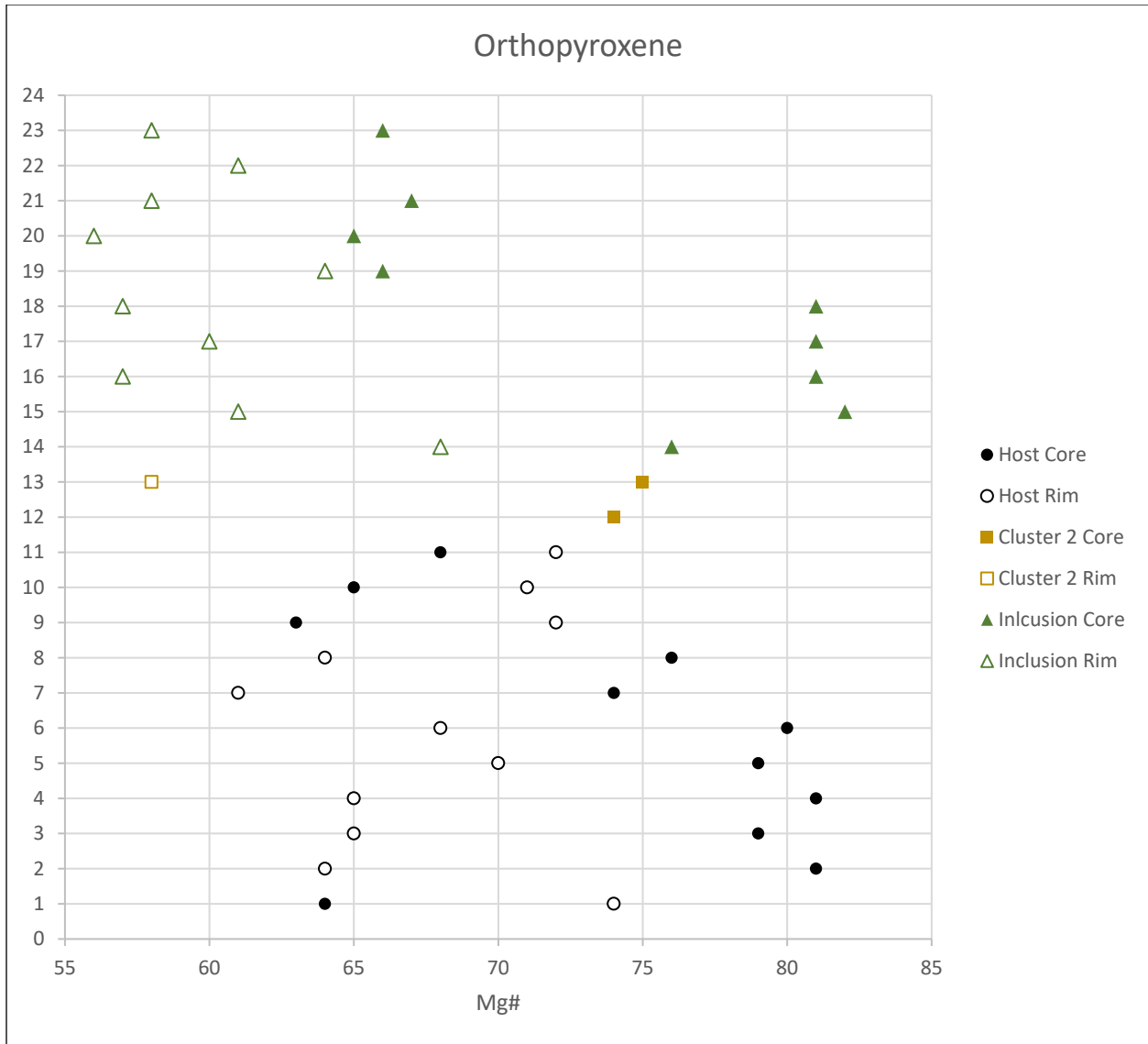


Figure 13. Orthopyroxene core and rim Mg# of analyzed crystals, with each line representing a single crystal. Dark, filled in shapes represent core data, and outlined shapes represent rim data. Host crystals are represented as black and grey circles. Cluster crystals are represented with orange diamonds (Cluster 1) and yellow squares (Cluster 2). Inclusion crystals are represented with green triangles.

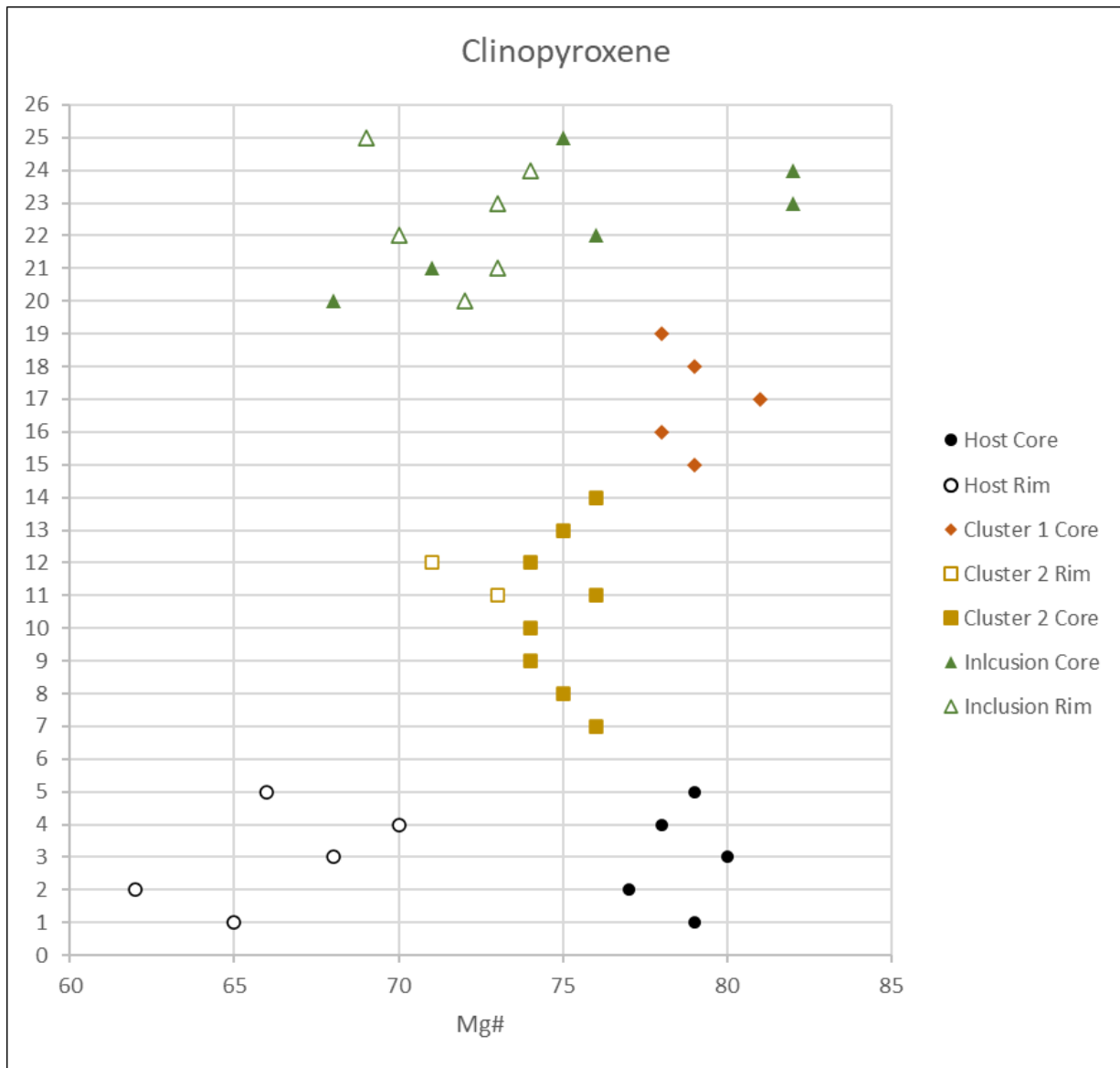


Figure 14. Clinopyroxene core and rim Mg# of analyzed crystals, with each line representing a single crystal. Dark, filled in shapes represent core data, and outlined shapes represent rim data. Host crystals are represented as black and grey circles. Cluster crystals are represented with orange diamonds (Cluster 1) and yellow squares (Cluster 2). Inclusion crystals are represented with green triangles.

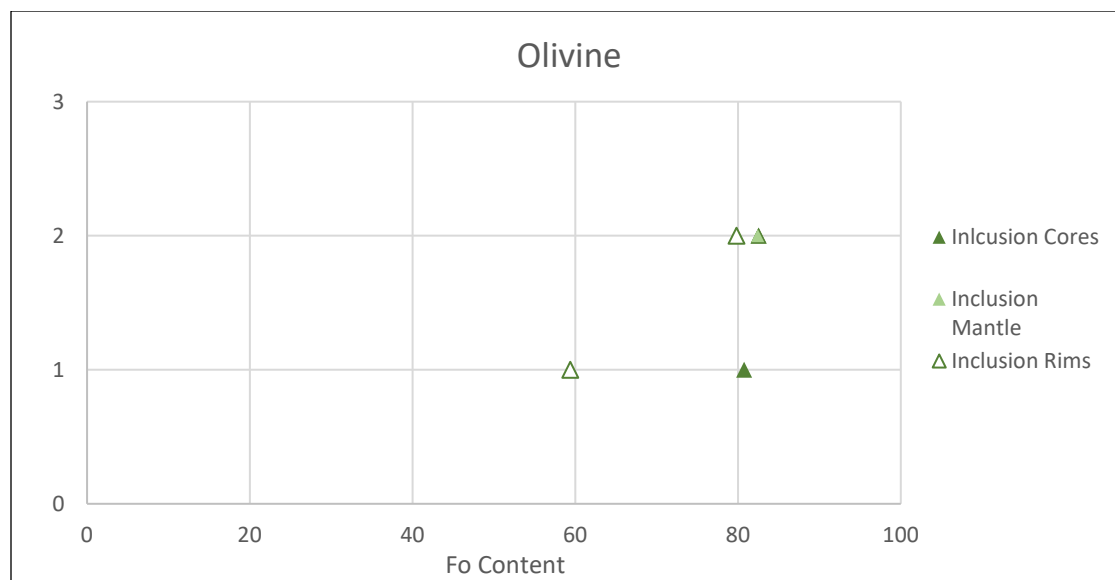


Figure 15. Olivine core, mantle and rim Fo contents of analyzed crystals, with each line representing a single crystal. Dark, filled in shapes represent core data, light, filled in shapes represent mantle data, and outlined shapes represent rim data. Inclusion crystals are represented with green triangles.

DISCUSSION

Mineral Populations

Plagioclase

In the host there are plagioclase crystals that are both normally and reversely zoned. The normally zoned plagioclase crystals have higher An core contents (An₇₅₋₉₁) than cores of reversely zoned plagioclase (An₅₇₋₆₂) (Fig. 12, Table 2). Rim An contents of both normally and reversely zoned plagioclase overlap and have a wider range than their respective cores. Specifically, rims of normally zoned crystals have An₆₃₋₈₁, and rims of reversely zoned crystals have An₆₅₋₈₁. A single mantle analysis of a normally zoned crystal had An₆₀, suggesting that normally zoned crystals could exhibit slight to moderate reverse zoning between the mantles and rims. Mantles of reversely zoned crystals had An₅₆₋₅₉, and have the same or lower An contents as their respective cores. There was no obvious correlation between size and compositional zoning as both normally and reversely zoned host plagioclase crystals varied in size. Since there is significant overlap between core, mantle, and rim An contents of all host plagioclase, the crystals may represent one population at with crystals that crystallized at different times (population Plg-H). Alternatively, there may be two populations of plagioclase. It should be mentioned that sieving was difficult to see in BSE imaging and therefore could not be associated with a specific compositional zoning.

Plagioclase crystals found in clusters indicate two distinct groups based on their core An contents, size, and associated cluster minerals. One group (Cluster 1) has larger crystals (≤ 0.5 mm) with higher An (82–83) and is found in clusters with higher Mg# (79–81) clinopyroxene. The second group (Cluster 2) has

smaller crystals ($\leq 50 \mu\text{m}$) with lower An (6–23) and is found in clusters with orthopyroxene (Mg#_{58–75}) and slightly lower Mg# clinopyroxene (73–76). These data suggest that two populations of plagioclase are found in the mineral clusters, one with higher An plagioclase and higher Mg# clinopyroxene (population Plg-C1) and another with lower An plagioclase, lower Mg# clinopyroxene, and orthopyroxene (population Plg-C2).

Inclusion plagioclase crystals all show normal zoning, but with a wider range of core and rim An contents relative to host and cluster plagioclase crystals (Fig. 12, Table 2). Core An contents are 51–78. Rim An contents appear to be in two discrete groups, one with moderate An contents of 23–39, and the other with lower An contents of 8–11. There is no correlation between the moderate and lower An rims and specific core An contents, and the crystals are all similarly sized and exhibit the same textures. These observations suggest a single population of plagioclase crystals whose rims may have crystallized across a wider time span and/or in melts with different compositions (population Plg-I).

Orthopyroxene

Host orthopyroxene crystals are as both normally zoned and reversely zoned, despite being identical in size and textures. The normally zoned cores have Mg#_{74–81} and their rims have Mg#_{61–70}. The reversely zoned crystals have core Mg#_{63–68} and rim Mg#_{71–74}. These observations suggest one population of orthopyroxene in the host that crystallized at different times (population Opx-H).

Orthopyroxene crystals found in clusters are normally zoned and exhibit the same size and textures. Core Mg# are 74–75 and a single rim analysis yielded Mg#₅₈. Orthopyroxene crystals in clusters are found with lower core An plagioclase (6–23) and lower core Mg# clinopyroxene (73–76) (Cluster 2). These observations suggest there is only one population of orthopyroxene found in the clusters (population Opx-C2).

Orthopyroxene crystals found in the inclusion have two distinct core Mg# groups but are the same in terms of size and textures. The first group of orthopyroxene cores have Mg#_{76–82}, and the second group have Mg#_{56–67}. For both core groups, the rim Mg# contents are 56–61, with one outlier at 64. These data suggest one population that crystallized at different times and/or was impacted by different degrees of magma mixing (population Opx-I).

Clinopyroxene

Host clinopyroxenes are all normally zoned and similar in composition. Core Mg# are 77–80 and rim Mg# are 62–70. Host clinopyroxene crystals range slightly in size but are texturally identical. These observations suggest one population of clinopyroxene in the host (population Cpx-H).

Clinopyroxene crystals found in clusters have a wide range of core Mg# and higher Mg# rims (relative to the host) but all crystals still only show normal zoning. Core Mg# are 74–81 and rim Mg# are 72–73. Cluster clinopyroxene crystals vary in size but are texturally identical. However, only higher core Mg# clinopyroxene crystals (79–81) are found in clusters with higher An plagioclase (82–83) (Cluster 1), and only lower core Mg# clinopyroxene are found in clusters with lower An plagioclase (6–23) and orthopyroxene (Cluster 2). These observations suggest the presence of two cluster clinopyroxene populations (higher core Mg#, population Cpx-C1; lower core Mg#, Cpx-C2).

Clinopyroxene crystals found in the inclusion show both normal and reverse zoning. Normally zoned core Mg# are 75–82 and their rim Mg# are 69–74. Reversely zoned cores have Mg#_{68–71} and their rims

have Mg#₇₂₋₇₃. Clinopyroxene crystals in the inclusion were texturally identical and similarly sized, although normally zoned clinopyroxene could be larger (>150 μm). These observations suggest one population of clinopyroxene that was impacted by different degrees of magma mixing and/or different crystallization timelines (population Cpx-I).

Olivine

Inclusion olivine crystals are normally zoned. The olivine cores have Fo₈₁₋₈₂ and rims Fo₅₉₋₈₀. The olivine crystals are identical in texture and size and likely represent a single population (population Oliv-I).

Amphibole

Although no compositions were obtained for amphiboles, there were two textural groups of amphibole present in the thin sections. The first group is euhedral-subhedral, simply twinned, and has a prominent oxidation ring. The second group consists of subhedral-anhedral amphibole crystals that reacted into clinopyroxene; the severity of the reaction of the second group varied throughout samples but was always distinct (more reacted) from the first group of amphiboles. Amphiboles in the first group are typically smaller than reacted amphiboles in the second group. The amphibole crystals either represent two populations or a single population with varying degrees of reaction due to difference degrees of interaction with a mafic component (Amp-H).

Quartz

Rare quartz crystals are found in the host or on the boundary between the host and inclusion and have a reaction rim of clinopyroxene microcrystals. Quartz crystals likely represent a single population (Qtz-H).

Correlating Mineral Populations and Their Potential Host Magmas

Host Minerals

The host magma is felsic-intermediate in composition based on mineral populations and their compositions. Populations Plg-H, Opx-H, Cpx-H, Amp-H, and Qtz-H all likely crystallized in the host, with Plg-H, Opx-H, Amp-H, and Qtz-H crystallizing before interaction with a mafic component and Cpx-H crystallizing after interaction. Populations Plg-H and Opx-H likely formed before the introduction of the mafic component, forming the lower An and lower Mg# cores of the reversely zoned crystals. After the mafic component was introduced, the lower An and lower Mg# cores continued crystallizing resulting in higher An and higher Mg# rims. At the same time, higher An and Mg# cores began to crystallize, these cores would then become the normally zoned host plagioclase and orthopyroxene crystals. Qtz-H and Amp-H likely also crystallized in the host before a mafic component was introduced. After the mafic component was introduced populations Qtz-H and Amp-H became unstable and started reacting into clinopyroxene. Population Cpx-H likely formed after the introduction of a mafic component. This is suggested because there is no evidence of disequilibrium and because both Qtz-H and Amp-H react into clinopyroxene indicating it became a stable phase after the mafic component was introduced.

Cluster Minerals

Populations Plg-C1 and Cpx-C1 are associated with one another, and both exhibit compositional and textural overlap with Plg-H and Cpx-H, respectfully. Therefore, Plg-C1 and Cpx-C1 are likely derived from

the host magma after the host magma interacted with a mafic component and are the same as Plg-H and Cpx-H, respectively.

Populations Plg-C2, Opx-C2, and Cpx-C2 are associated with each other. These populations do not exhibit an obvious association with either the host populations or the inclusion populations. It is possible that they are instead sourced from some third intermediate component.

Inclusion Minerals

The inclusion is compositionally mafic based on mineral populations and their compositions. The inclusion is representative of the mafic component introduced to the host magma. Population Olv-I likely formed in the inclusion before interaction with the host as indicated by high Fo cores as well as textural evidence of disequilibrium (dominantly subhedral in shape). Populations Plg-I, Opx-I, and Cpx-I likely crystallized after interaction with the host magma and exhibit a wide array of core and rim compositions. The wide array of core and rim compositions is because the degree of mixing between these two magmas varied on a local scale as evidenced by the size, distribution, and abundance of mafic inclusion blebs.

Summary and Sequence of Events

Populations Plg-H, Opx-H, Amp-H, Qtz-H, and Olv-I all likely crystallized in their respective host magmas before the magmas interacted. Following magma mingling, Plg-H and Opx-H continued to crystallize, resulting in reversely zoned crystals, and also started growing new crystals, resulting in normally zoned crystals. Amp-H, Qtz-H, and Olv-I became unstable and started to break down, and the extent of their individual crystal reactions varied depending on the local extent of mixing between the host and inclusion. Populations Plg-I, Opx-I and Cpx-I all crystallized following magma mingling, and their wide range of compositions is a result of observed variable extent of localized mixing between the host and inclusion. Cluster 2 crystals (populations Plg-C2, Opx-C2, and Cpx-C2) have unclear origins. Their compositions do not show any obvious correlation to either the host or the inclusion and as such are likely sourced from some third source. The clusters are more commonly found in the inclusion, and therefore may have been picked up by the inclusion shortly before the magmas mingled as there is no apparent reverse zoning in Cluster 2 crystals. The populations in the inclusion and host that crystallized after the host and inclusion mingled (Cpx-H, Plg-I, Opx-I, and Cpx-I) indicate the interaction of the magmas did not trigger the eruption (the populations had time to crystallize and establish themselves). There is no definitive evidence for what resulted in the eruption. However, the host has a microcrystalline, glassy matrix, suggesting the addition of a phenocryst-free liquid before eruption. This means that a second intrusion event had to have taken place after the initial mafic inclusion to remobilize the crystallized, mingled magmas.

CONCLUSION

Understanding which magmatic processes occur at volcanic sites offers valuable insight into pre-eruptive activity. Dahkobod/Glacier Peak is a Cascade volcano whose magmatic system is not well

understood. In hopes of better understanding magmatic processes at Glacier Peak, numerous samples of Glacier Peak dacite were studied petrographically and analyzed using FE-SEM. Samples consisted of two mingled magmas, a felsic-intermediate host and a mafic inclusion. It was determined that four populations of minerals crystallized in the host (Plg-H, Opx-H, Amp-H, Qtz-H) and one population crystallized in the inclusion (Olv-I) prior to magma interaction. Following mingling, several mineral populations became unstable (Amp-H, Qtz-H, Olv-I), while others continued to crystallize and nucleate (Plg-H, Opx-H), and new populations started growing in both the host (Cpx-H) and inclusion (Plg-I, Cpx-I, Opx-I). A third magmatic component is needed to explain three mineral populations found together in clusters (Plg-C2, Opx-C2, Cpx-C2). This third component is intermediate in composition, volumetrically smaller than the host and inclusion, and derived from an unknown source. However, since the clusters are more commonly found in the inclusion, it is possible that this third component was picked up by the inclusion shortly prior to interaction with the host magma. Since there is evidence for extensive crystallization and re-crystallization after the host and inclusion magmas interacted, it is unlikely that this mixing event was the trigger for eruption. The mingled magma stagnated long enough for the inclusion matrix to fully crystallize, but another intrusion event likely took place for the magma to be remobilized before the host matrix. This event may have been a second intrusion of mafic magma to the system but requires further research to confirm.

FUTURE WORK

In the future it would be valuable to analyze the glass and microphenocryst compositions of the host magma. If the trigger for eruption was the introduction of a different magma, it would most be reflected in the glass and microphenocrysts of the host matrix. Additionally, using laser ablation inductively-coupled plasma mass spectrometry (LA-ICP-MS) to measure trace element concentrations in minerals would help refine and distinguish the mineral populations and may lead to greater insight about the magmatic system and potential sources.

ACKNOWLEDGEMENTS

I acknowledge that Dahkobod/Glacier Peak is located in the ancestral homelands of the Sauk Suiattle Tribe. I would like to express my respect, gratitude, and appreciation for the Sauk Suiattle Tribe. I would like to thank Dr. Susan DeBari for providing me with the samples. I would like to thank Dr. Mike Kraft for all his help navigating and operating the SEM both digitally and in person. I would like to thank Ben Paulson for all the work he did to minimize COVID risks while researching and all of his ongoing support. I would like to thank Dr. Mai Sas who has been there for me with every twist and turn over the last two years and whose sage words and advice I will remember for a lifetime. I would like to thank Conor O'Leary for his unbridled support and enthusiasm, I could not have made it without you.

REFERENCES

- Bebout, G.E., 2013. Volatile Transfer and Recycling at Convergent Margins: Mass-Balance and Insights from High-P/T Metamorphic Rocks, in: Bebout, G.E., Scholl, D.W., Kirby, S.H., Platt, J.P. (Eds.), *Geophysical Monograph Series*. American Geophysical Union, Washington, D. C., pp. 179–193.
<https://doi.org/10.1029/GM096p0179>

- Beget, J.E., 1983. Glacier Peak, Washington: A potentially hazardous cascade volcano. *Environmental Geology* 5, 83–92. <https://doi.org/10.1007/BF02381101>
- DiPietro, J.A., 2018. Chapter 19 - Cascadia Volcanic Arc System, in: DiPietro, J.A. (Ed.), *Geology and Landscape Evolution* (Second Edition). Elsevier, pp. 473–499. <https://doi.org/10.1016/B978-0-12-811191-8.00019-1>
- Escobar-Burciaga, R.D., 2016. Mineral Complexities as Evidence for Open-system Processes in Formation of Intermediate Magmas of the Mount Baker Volcanic Field, Northern Cascade Arc. M.S. Thesis, Western Washington University 173.
- Leeman, W.P., Smith, D.R., 2018. The role of magma mixing, identification of mafic magma inputs, and structure of the underlying magmatic system at Mount St. Helens. *American Mineralogist* 103, 1925–1944. <https://doi.org/10.2138/am-2018-6555>
- McCrory, P.A., Blair, J.L., Waldhauser, F., Oppenheimer, D.H., 2012. Juan de Fuca slab geometry and its relation to Wadati-Benioff zone seismicity. *Journal of Geophysical Research: Solid Earth* 117, B09306. <https://doi.org/10.1029/2012JB009407>
- Mullen, E.K., Weis, D., 2015. Evidence for trench-parallel mantle flow in the northern Cascade Arc from basalt geochemistry. *Earth and Planetary Science Letters* 414, 100–107. <https://doi.org/10.1016/j.epsl.2015.01.010>
- Sas, M., DeBari, Susan, Clynne, Michael, 2017. Using mineral geochemistry to decipher slab, mantle, and crustal input in the generation of high-Mg andesites and basaltic andesites from the northern Cascade Arc. *American Mineralogist* 102, 948-965. <https://doi.org/10.2138/am-2017-5756>
- Sparks, R.S.J., Annen, C., Blundy, J.D., Cashman, K.V., Rust, A.C., Jackson, M.D., 2019. Formation and dynamics of magma reservoirs. *Philosophical Transactions of the Royal Society A: Mathematical, Physical and Engineering Sciences* 377, 20180019. <http://dx.doi.org/10.1098/rsta.2018.0019>
- Streck, M.J., 2008. Mineral Textures and Zoning as Evidence for Open System Processes. *Reviews in Mineralogy and Geochemistry* 69, 595–622. <https://doi.org/10.2138/rmg.2008.69.15>
- Syracuse, E.M., van Keken, P.E., Abers, G.A., 2010. The global range of subduction zone thermal models. *Physics of the Earth and Planetary Interiors, Special Issue on Deep Slab and Mantle Dynamics* 183, 73–90. <https://doi.org/10.1016/j.pepi.2010.02.004>
- United States Geologic Survey, 2018. Glacier Peak Geology and History [WWW Document]. URL https://www.usgs.gov/volcanoes/glacier-peak/geology-and-history?qt-science_support_page_related_con=4#qt-science_support_page_related_con (accessed 2.19.21).